Article

Patterns of Reacted Adatoms in Adsorption of Acetonitrile on Si{111}-(7 × 7)

Hironori Mizutani, Hyeong-Kyu Choi, Jinwoo Park, Suklyun Hong,* and Michio Okada*

Read Online

| ACCESS | | Metrics & More | | Article Recommendations | | Supporting Information |

ABSTRACT: We report on the covalent binding of acetonitrile (CH_3CN) on Si{111}-(7 × 7) at ~300 K studied by scanning tunneling microscopy, thermal desorption spectroscopy, and first-principles theoretical calculations. The site-specific study makes it possible to unravel the site-by-site and step-by-step kinetics. A polarized CH_3CN prefers to adsorb on the faulted half more frequently compared to on the unfaulted half. Moreover, a molecular CH_3CN adsorbs four-times more preferably on the center adatom-rest atom (CEA-REA) pair than on the corner adatom-rest atom (COA-REA) pair. Such site selectivity, the number ratio of reacted-CEA/reacted-COA, depends on the number of reacted adatoms in the half-unit cell. The site selectivity and the resulting reacted-adatom patterns are understood well by considering a simple model. In this simple model, the molecular adsorption probability changes step-by-step and site-by-site with increasing reacted adatoms. Furthermore, our theoretical calculations are overall consistent with the experimental results. The site-selectivity of the adsorption of CH_3CN on Si{111}-(7 × 7) is explained well by the chemical reactivity depending on the local conformation, the local density of states, and the interaction between polarized adsorbates.
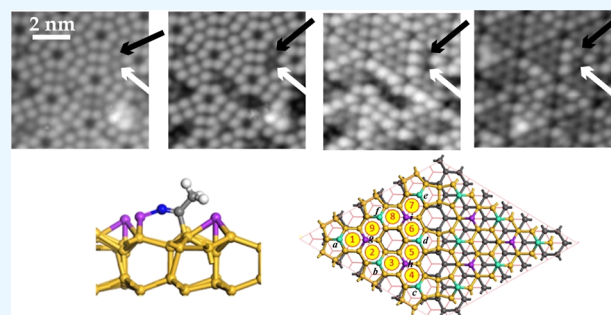
1. INTRODUCTION

Although new concepts of microelectronics have been developed in various technologies today, silicon still plays a unique role in the development of various kinds of semiconductor devices. Studies on silicon-based surface chemistry have attracted a lot of attention from the perspective of basic science.[1−7] A lot of research works have been performed for the molecular adsorption on Si surfaces,[8−37] where the various types of molecules, from simple to complex ones, are used for exploring new functions of surfaces. Several works have concerned mainly on the molecules with unpolarized C≡C or C=C,[8−12] multiple-membered aromatics,[13−15,29,30] some unsaturated cyclic hydrocarbons,[16,17,36] zwitterionic organic molecules,[31,32] and benzene and its related molecules.[18−21,28,31−35] The adsorption behavior of polarized molecules with C≡N function, the simplest nitrile of acetonitrile, was reported on Si{100}.[22−26] For acetonitrile, it was suggested in several experimental[22,23] and theoretical[22,24−26] works that a [2 + 2] cycloaddition reaction through the C≡N function occurred (di-σ model). The acetonitrile adsorbed molecularly on Si{100} in a di-σ configuration, holding a C=N functionality, followed by further multiple reactions.[22−26]

It is expected that a relatively simple adsorption mechanism occurs on Si{111}-(7 × 7), primarily involving the adatom-rest-atom pair behaving as a diradical (electrophilic and nucleophilic atoms). The Si{111}-(7 × 7) is schematically represented in Figure 1a.[38]

The 19 dangling bonds are located at 7 spatially inequivalent types of Si atoms of Si{111}-(7 × 7), i.e., corner adatoms (COAs), center adatoms (CEAs), and rest atoms (REAs) on both faulted and unfaulted halves and the corner-hole atom (CHA).[39] Each REA or CHA has a formal charge of −1. On the other hand, each adatom has an electron occupancy of 5/12, resulting in a formal charge of about +7/12. Moreover, two neighboring REAs are related to each CEA, while each COA has only one neighboring REA. The charge transfer from the CEA to the REA amounts to roughly twice as much as that from the COA. As a result, the COA possesses higher electron density than the CEA, inducing their difference in the chemical reactivity. Thus, the Si{111}-(7 × 7) surface is much polarized. The inherent electronic differences of these atoms are readily observable in the STM image in Figure 1b.

The combination of the functional polarity of a molecule with an unsaturated bond and the electronically inequivalence of the surface dangling bonds of the Si{111} gives an arising of interesting chemistry. Acetonitrile is a candidate because of the simplest nitrile having a large dipole moment of 3.92 D.[40]
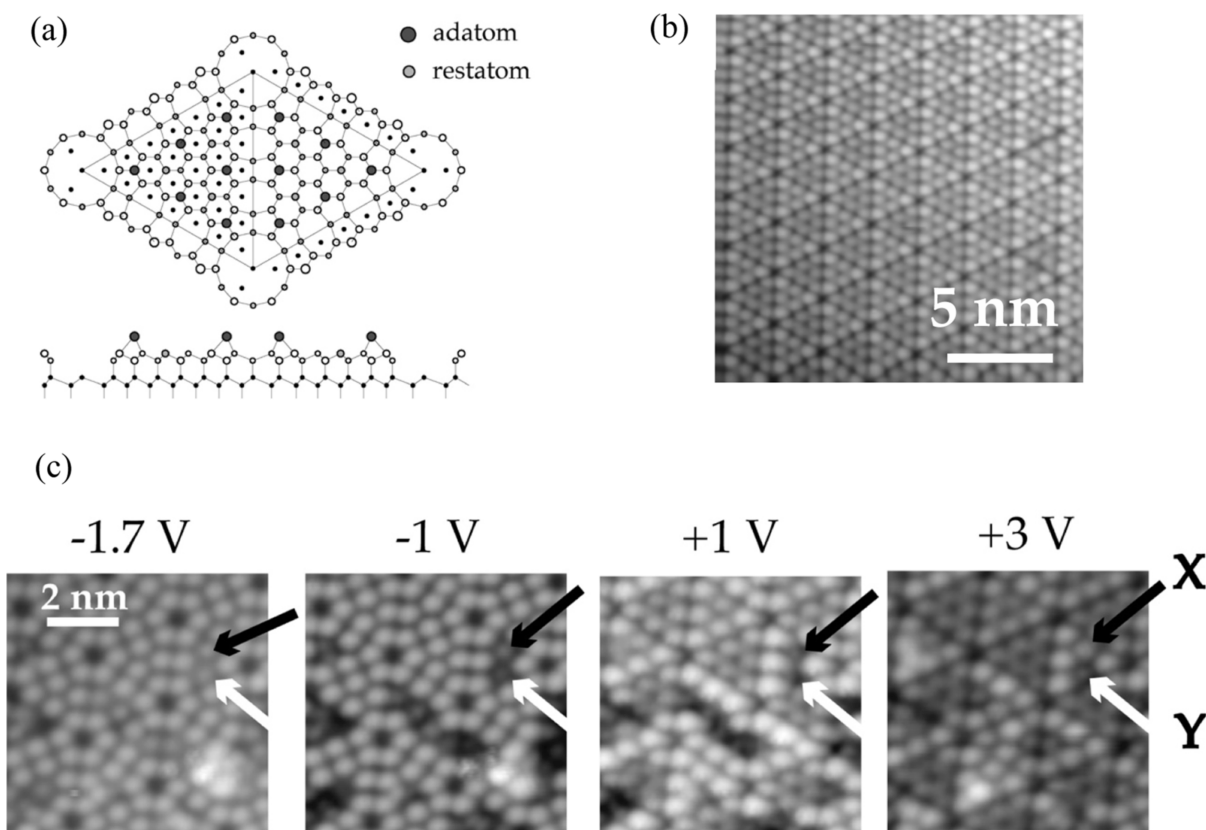
Figure 1. (a) Dimer adatom stacking fault model of the Si{111}-(7 × 7). (b) Topographic image of clean Si{111}, which was measured at the tip bias of +1.7 with a tunneling current of 0.25 nA at room temperature. (c) Tip-bias dependence of topographic images for the 3 L-CH$_3$CN exposure on Si{111}-(7 × 7) at ∼300 K, obtained at the tip bias of −1.7−1.0, +1.0, and +3.0 V with a constant 0.25 nA tunneling current, respectively. Type X and Y adatoms are indicated by black and white arrows, respectively (see text). Reproduced with permission from ref 43 Copyright 2021 American Chemical Society.

It was reported that the acetonitrile was adsorbed on Si{111}-(7 × 7) through a di-σ bonding involving the coupling of an adatom-rest atom pair and the π_{CN}.[41] The slight dissociation of CH$_3$CN on Si{111} was also reported.[42] Recent work of scanning tunneling microscopy (STM) and density functional theory (DFT) calculations suggests that the acetonitrile on Si{111}-(7 × 7) may also have a more complex aspect than explained only by the molecular chemisorption.[43] In the present paper, we report the site-by-site and step-by-step adsorption of CH$_3$CN on Si{111}-(7 × 7) by analyzing the reacted-adatom patterns measured by STM and their related theoretical calculations. We found that the adsorption of CH$_3$CN on Si{111}-(7 × 7) can be described well by the model involving the formation probability of various reacted-adatom patterns. Then, it is concluded that the adsorption of CH$_3$CN on Si{111} depends on the local conformation of the chemical bonds, the adsorbate−adsorbate interaction, and the local density of states (LDOS) of surface atoms.

2. EXPERIMENTAL AND CALCULATIONAL METHODS

The vacuum system consists of two UHV chambers; one chamber for the preparation of the samples as well as to their exposure to CH$_3$CN, and the other for the scanning tunneling microscope (UMS-901S, UNISOKU Co.) and quadrupole mass spectrometer for thermal desorption spectroscopy (TDS). The base pressure of both chambers is below 1 × 10^{-8} Pa. We measured the STM images at ∼300 K with a tip made of Pt−Ir. The CH$_3$CN gas was introduced into the UHV

chamber after purification with freeze−pump−thaw cycles. The purification of CH$_3$CN was confirmed by the quadrupole mass spectrometer.

The Si{111} (P-doped n-type, 0.4−0.6 Ω cm^{-1}) sample mounted on the Mo sample holder was cleaned by heating it to 1473 K repeatedly. The density of the defects on the Si{111}-(7 × 7) surface amounts to less than 0.5% after the sample cleaning.

We performed first-principles calculations using the Vienna ab initio simulation package (VASP) to study the configuration of CH$_3$CN on Si{111}-(7 × 7).[44,45] The Perdew−Burke−Ernzerhof (PBE) functional in the generalized gradient approximation (GGA)[46] was employed for exchange−correlation electron interactions. Electron−ion interactions were described using the projector augmented-wave (PAW) method with a plane wave basis set and a cutoff energy of 400 eV.[47,48] van der Waals (vdW) corrections were accounted for using Grimme's DFT-D3 approach.[49]

The Si{111}-(7 × 7) surface with CH$_3$CN adsorption was modeled by a slab using a supercell, which includes adsorbed CH$_3$CN molecules, seven Si atomic layers (including one adatom layer), and a H passivating layer. The dimer−adatom−stacking fault (DAS) model, as shown in Figure 1a,[27,50] was used to describe Si{111}-(7 × 7). During the optimization, the bottom H atom layer and two Si atom layers were fixed, while the other Si atoms and CH$_3$CN molecules were allowed to relax. The optimized surface structure reached equilibrium when the Hellman−Feynman force was less than 0.02 eV/Å.

For Brillouin-zone integration, we used a $3 \times 3 \times 1$ grid in the Monkhorst−Pack special point scheme. Gaussian broadening with a width of 0.02 eV was employed to accelerate convergence in the k-point sum. The asymmetric slab model was used to consider the dipole corrections.

3. RESULTS AND DISCUSSION

3.1. CH$_3$CN Configurations on Si{111}-(7 × 7).
The CH$_3$CN-coverage dependence of STM images measured on
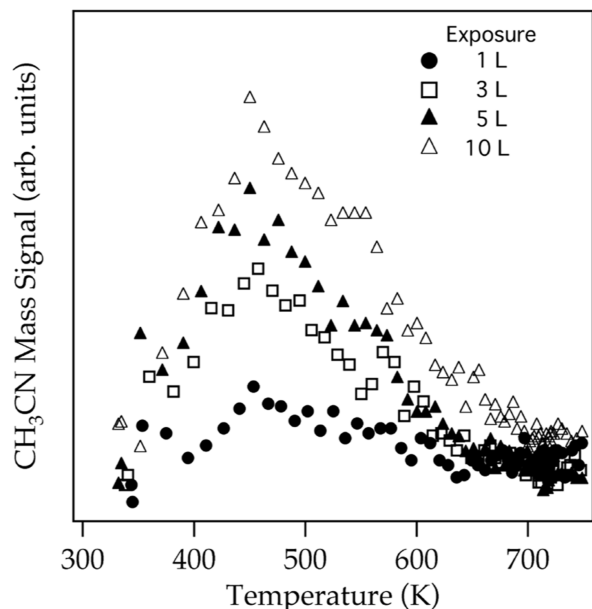
Figure 2. Thermal desorption spectra of CH$_3$CN on Si{111} for 1, 3, 5, and 10 L exposures.
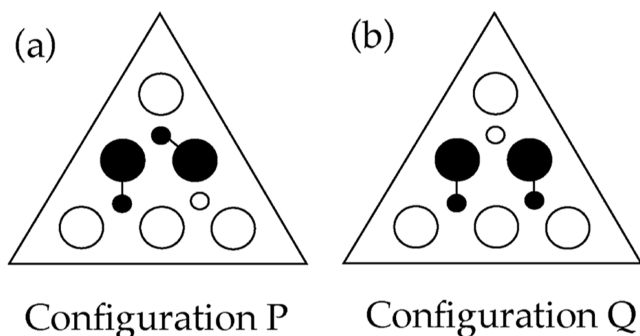
Figure 3. Schematic ball models of CH$_3$CN chemisorbed on Si{111}-(7 × 7) for configurations (a) P and (b) Q. CH$_3$CN chemisorbed adatoms and the remaining atoms are indicated with black circles. The pair of adjacent adatoms and rest atoms occupied by the CH$_3$CN chemisorption (including its derivatives) is connected by a line.

Si{111} at ~300 K was already reported elsewhere.[43] Figure 1c demonstrates the tip-bias dependence of the topographic image at the 3 L (1 L = 1.33×10^{-4} Pa s) CH$_3$CN exposure on Si{111}.[43] The dark appearance of adatoms at the tip bias of +1.0 V is classified into several types. One is the CEA (denoted by X) that becomes bright at the tip bias of +3.0 V. The brightness was similar to that of the nonreacted adatoms. The second is the CEA (denoted by Y) that stays dark even at the tip bias of +3.0 V. The others are also stated in ref 43. The X adatom makes a pair most likely with the Y adatom. The pair of Y adatoms was rarely observed, and their population is
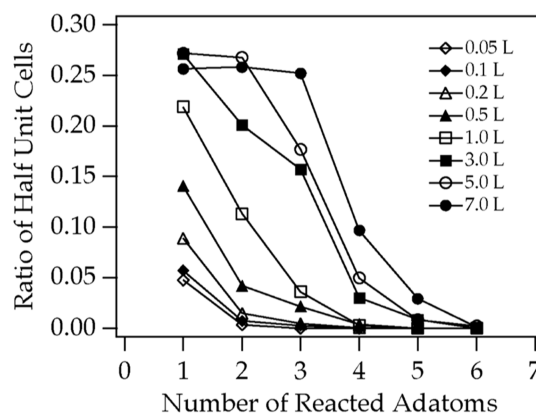
Figure 4. Reacted-adatom-number dependence of the distributions of half-unit cells on CH$_3$CN chemisorbed Si{111}-(7 × 7), measured with varying the CH$_3$CN exposure.
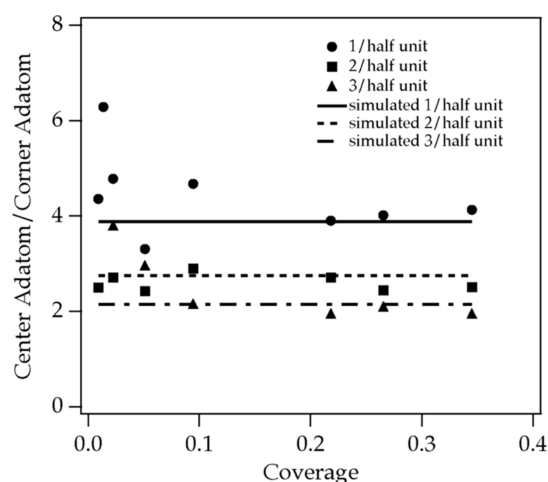
Figure 5. Center-to-corner population ratio of the reacted adatoms. Experimental data for 1, 2, and 3 reacted adatoms in a half-unit cell are indicated with circles, squares, and triangles, respectively. The corresponding simulations are shown as full, dashed, and dotted lines, respectively (see text). Center-to-corner population ratio of the reacted adatoms takes individual constant values depending on the number of reacted adatoms in a half-unit cell.

about 10% of the X−Y pair. No pair of X adatoms was observed.

Although the populations of CEAs X and Y are large, the very recent theoretical calculations of STM image failed to assign them to the specific molecular species and structures,[43] where the STM image of an isolated reacted site is calculated and discussed. Taking the most possible di-σ bonding of CN to the pair of an adatom and an adjacent rest atom into consideration, it is reasonable that the adsorption occurs on the pair, resulting in the reacted-adatoms-pattern formation. The previous report[41] demonstrated the various spectroscopic evidence of C≡N and C−C of CH$_3$CN on Si{111}. Furthermore, thermal desorption spectroscopy (TDS) demonstrates the significant *molecular* CH$_3$CN desorption in Figure 2, suggesting the molecularly adsorbed species for X and Y. Therefore, we assume that the X + Y pair configuration occurs dominantly in molecular CH$_3$CN adsorption.

Two possible configurations can be considered for the two reacted CEAs in a half-unit cell, as demonstrated in Figure 3, depending on the selection of a pair of CEA and REA. For
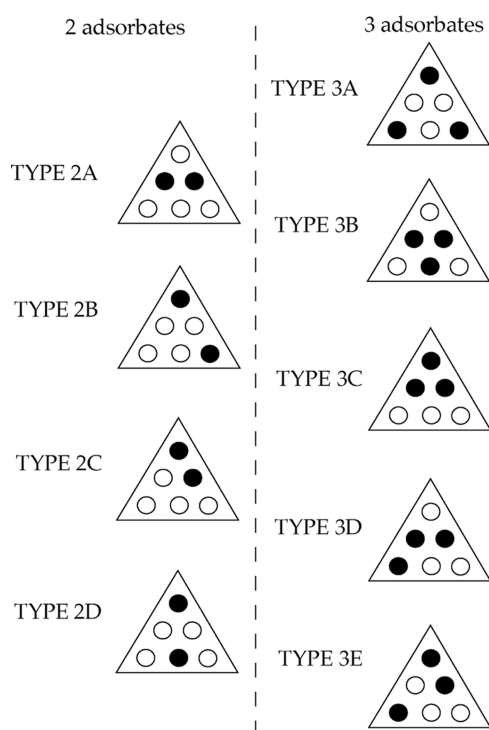
Figure 6. Adsorption patterns for 2 and 3 adsorbates on a half-unit cell in the left and right panels.
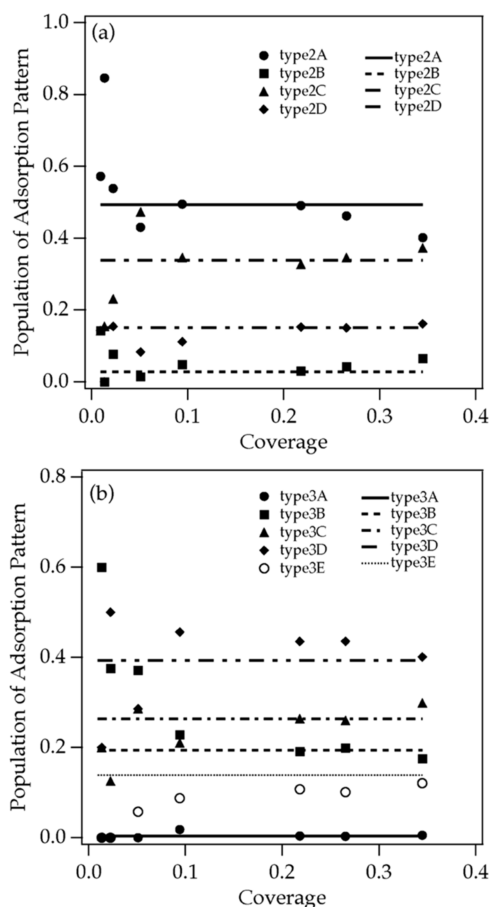
Figure 7. Formation probability of adsorption pattern in Figure 6 for (a) 2 adsorbates and (b) 3 adsorbates. Markers and lines correspond to the experimental data and simulations (see text).

configuration P in Figure 3, one of the reacted CEAs is surrounded by the two reacted REAs, while the other is surrounded by one. Considering the charge redistribution due to the adsorption of a strongly polarized CH_3CN, the two CEAs may possess possibly different charge density. As a result, the tip-bias dependence of the STM image appears differently on the two reacted center adatoms. On the other hand, for the configuration Q in Figure 3, the surroundings of the two reacted CEAs are the same, and thus, the same tip-bias dependence of the CEA appearance is expected. The long-range dipole−dipole interaction between the polarized molecules may reduce the population of the configuration Q. Here, we assume P and Q having a most stable geometry of an adsorbed CH_3CN with the C and N atoms bonded to the rest atom and the nearest adatom, respectively.[43] (Note that configurations P and Q are described without distinction as type 2A in Figure 6 below. More specifically, P and Q are denoted as types 2A and 2A* in Table 1.)

Figure 4 demonstrates the CH_3CN-exposure dependence of the distribution of the half-unit cells having reacted adatoms. If the adsorption of CH_3CN is limited only on the adjacent pair of an adatom and a rest atom, it is expected that the maximum number of reacted adatoms in a half-unit cell is three. About 10% of the reacted half-unit cells contain more than 4 reacted adatoms. The number of such half-unit cells is smaller in the unfaulted halve than in the faulted halves and is also larger than anticipated from the number of pre-existing defects, suggesting the dissociation of some part of CH_3CN, possibly into CH_2CN and H[42,43,51] and/or further dissociation.

3.2. Site-Selectivity of CH_3CN on Si{111}-(7 × 7). A statistical counting of reacted adatoms elucidates the site selectivity in the acetonitrile adsorption, as already discussed in ref 43. It is evident from the CH_3CN-uptake curves obtained by the STM that CH_3CN adsorbs preferably on the faulted half of the unit cell.[43] The LDOS of adatoms in which the stacking fault increases can be distinguished in the filled-state STM image. Compared to the total coverage of 0.42 (the coverage is defined as the ratio of the reacted adatoms to the total adatoms), about 61% of the reacted adatoms are in the faulted half, while 39% are in the unfaulted half. The slightly higher LDOS of the faulted halves may contribute to the higher reactivity.

The site selectivity, the number ratio of reacted-CEA/reacted-COA, depends on the CH_3CN coverage. As we reported previously,[43] the ratio of reacted-CEA/reacted-COA = 4 for the early stage of the exposure of CH_3CN, and it decreases from 4 to 2 monotonously with increasing exposure. The total coverage dependence of the ratio of reacted-CEA/reacted-COA obtained for each half-unit cell with the same number of reacted adatoms is shown in Figure 5. The ratio reveals a constant value of 4, 3, and 2, as demonstrated in Figure 5.

3.3. Kinetics of CH_3CN Adsorption on Si{111}-(7 × 7). Here, we consider the case that the adsorption of a CH_3CN occurs molecularly only on the pair of an adatom and its adjacent rest atom. The possible reacted-adatom patterns of type 2A ∼ 2D and type 3A ∼ 3E for the 2 and 3 CH_3CN adsorbates on a half-unit cell, respectively, are shown in Figure 6. The pattern-formation probability reveals remarkably constant values, which are independent of the total coverage of the reacted adatoms, as shown in Figure 7. Furthermore, the adsorption probability changes step-by-step and site-by-site
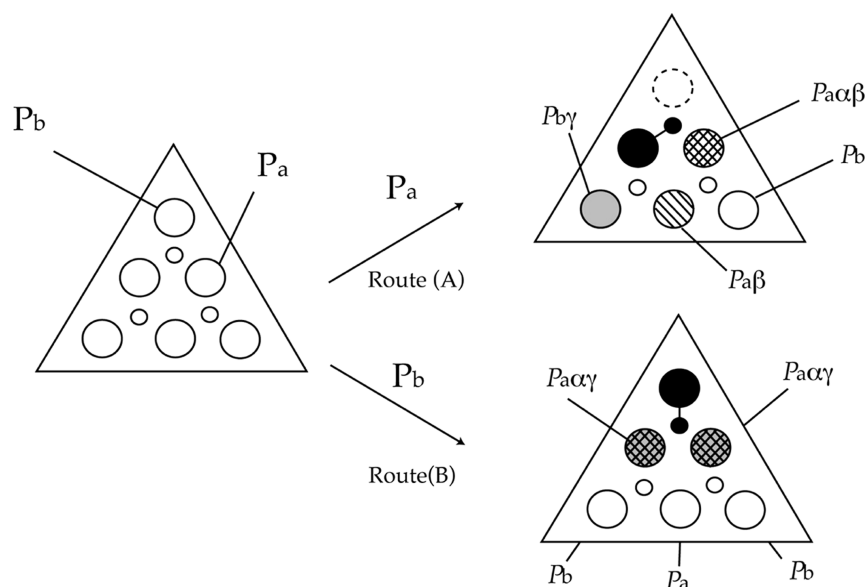
Figure 8. Adsorption pattern (right) for one CH_3CN in a half-unit cell. Adsorption probability of CH_3CN assuming the adsorption occurs only on a pair of an adatom and its nearest rest atom in a half-unit cell. P_a [route (A)] and P_b [route (B)] correspond to the adsorption probability for one of the CEAs and one of the COAs on the virgin Si{111} (left). Numerical expressions in the right panel represent the conditional probability for the adsorption of the second CH_3CN, where α is a parameter corresponding to local conformation and β and γ are parameters on the interaction induced by the nearest adsorbate (see also text). Large and small circles indicate the Si adatoms and rest atoms. Full-black and dashed circles indicate the reacted atoms and adatoms losing their capability of reactions, respectively. Cross-hatched and hatched circles indicate the nearest Si CEAs to the reacted CEAs, with and without changes in the conformation, respectively. Gray circles indicate the available COA nearest to the reacted CEA in route (A) and the available CEAs nearest to the reacted COA in route (B).

with increasing reacted adatoms, as shown in Figures 4, 5 and 7.

In the clean half-unit cell of Si{111}-(7 × 7), a CEA has two adjacent REAs, while a COA has one adjacent REA. The adsorption of CH_3CN occurs via either route (A) or (B), as described in Figure 8. The CH_3CN adsorbs at one of the CEA-REA pairs in route (A), while at one of the COA-REA pairs in route (B). Experimental observation demonstrates that the adsorption probability at the CEA-REA pair is about four times larger than that at the COA-REA pair site in the initial stage. The ratio of reacted-CEA/reacted-COA = 4 corresponds to the relative balance of the routes (A,B). Thus, the adsorption probability via route (A) is $P_a = 4/5$, while that via route (B) is $P_b = 1/5$. After the first adsorption of CH_3CN occurs on either a CEA or a COA, the number of REAs available for the second CH_3CN adsorption is 0−2, depending on the adatom position, as illustrated in Figure 8. When the first adsorption of a CH_3CN occurs in route (A), one of the COAs illustrated as a dashed circle is inevitably ruled out as a candidate for the second adsorption site because it has no available nearest REA, as shown in Figure 8. Moreover, a CEA described by the cross-hatched circle loses one adjacent REA. As a result, its local conformation is the same as that of the nonreacted COA. Therefore, the change in the LDOS and the local conformation induced by the first preadsorbed CH_3CN should be taken into account for the adsorption of the second CH_3CN. This kind of model simulation was quite successful for the dissociative adsorption of CH_3OH on Si{111}-(7 × 7),[52] and here we apply it to the present CH_3CN on Si{111}-(7 × 7).

We consider that both the local conformation (availability of REAs) and the LDOS of adatoms are responsible for the site selectivity, reacted-CEA/reacted-COA. As demonstrated in Figure 8, the probability for the adsorption of the second CH_3CN at the hatched CEA is given by $P_a\alpha\beta$, where α and β

are structural parameters depending on the local conformation of the CEA-REA pair and a parameter reflecting both the local interaction between the first and second CH_3CN on the CEAs and the related changes of the target adatom in LDOS, respectively. On the other hand, in the case of the first CH_3CN on the CEA and the second on its nearest COAs [see the gray circle in route (A) in Figure 8], we use a parameter γ in place of β. If the adsorption probability of the second CH_3CN does not depend on the local conformation change and on the interaction between adsorbates, then α and β (γ) would be equal to 1. On the other hand, if the adsorption probability strictly depends on the local conformation, α would be 0.5 for the cross-hatched adatom in Figure 8, because the number of remaining atoms available for the second adsorption becomes half. As such, the formulas of the site-by-site adsorption probability of the second CH_3CN can be derived in the route (A) as $P_a\alpha\beta$, P_b, $P_a\beta$, and $P_b\gamma$ for the possible five adatoms. Similarly, the reaction probability for the five adatoms in route (B) is given by $P_a\alpha\gamma$, $P_a\alpha\gamma$, P_a, P_b, and P_b. Five possible adsorption patterns appear after the adsorption of the second CH_3CN in route (A), as shown in Figure 9a (see the filled-black-atom patterns). It should be noted that one of the available CEAs has two REAs. On the other hand, the six adsorption patterns appear in route (B), as shown in Figure 9b (see the filled-black-atom patterns). The formation probability of each pattern of reacted adatoms is represented by the equations of $P_a \cdot Q_{nA}$ ($n = 1{-}5$) and $P_b \cdot Q_{nB}$ ($n = 1{-}5$), where Q_{nA} and Q_{nB} are the formation probability of each pattern in the condition of selection of routes (A,B), respectively. Here, a parameter of δ is introduced in Figure 9a, corresponding to the route selection (selection of one of two available REAs).

The chemisorption of the third CH_3CN demonstrates totally 10 and 16 saturated adsorption patterns in the route (A,B), as illustrated in Figure 10a,b, respectively. The available
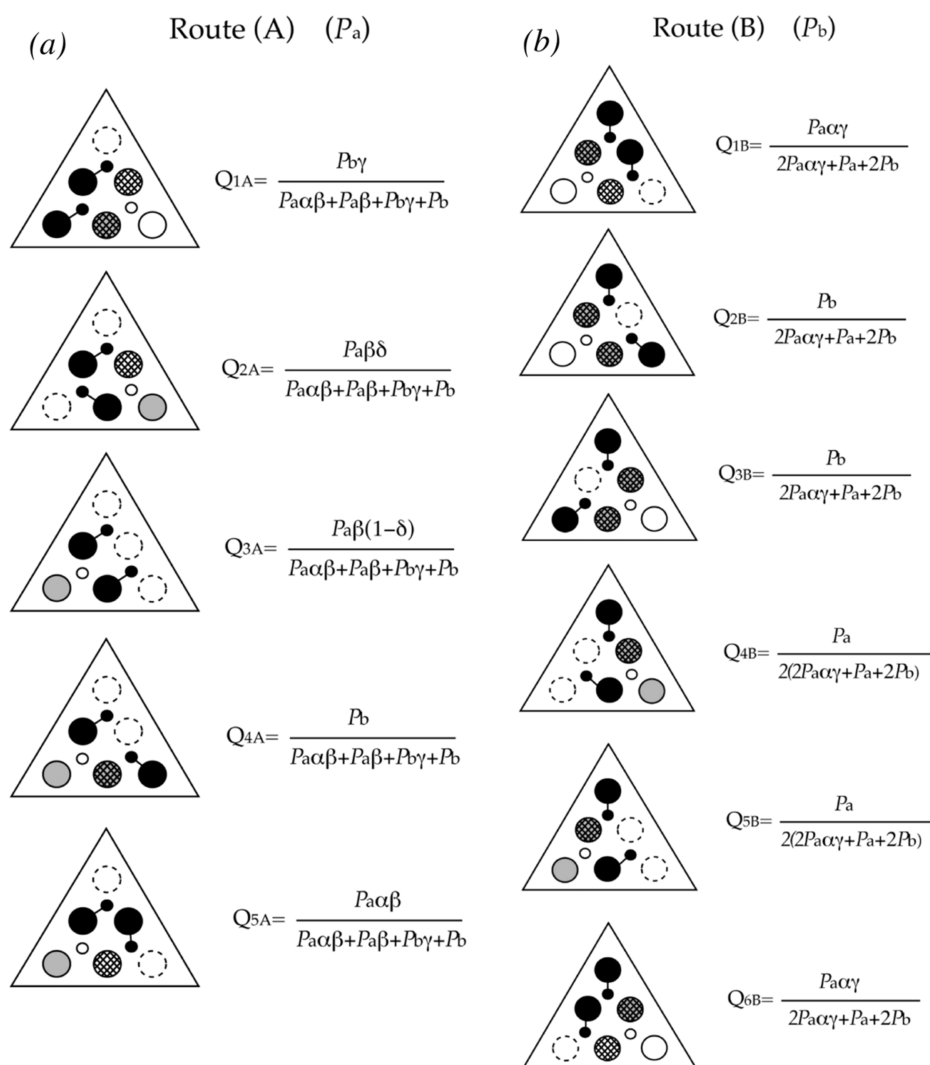
Figure 9. (a) Adsorption patterns of the Si adatoms and their formation probability in route (A). (b) Adsorption patterns of the Si adatoms and their formation probability in route (B). Q_{nA} ($n = 1-5$) and Q_{nB} ($n = 1-5$) are the formation probability of each pattern in the condition of selection of routes (A,B) in Figure 8, respectively.

adatoms for the third CH_3CN are marked in Figure 9 (similarly, most are left in Figure 10). The formation probability for each pattern for the third CH_3CN adsorption on the patterns for two CH_3CN in Figure 9 (most left in Figure 10) is described by the formula indicated below for each produced pattern shown in Figure 10. The local interaction of the third molecule with two preadsorbed CH_3CN molecules on the nearest adatoms should be considered. Here, we assume that interaction with the nearest CH_3CN molecule plays a dominant role. The overall pattern-formation probability for three CH_3CN groups can be calculated by the conditional probability of each pattern formation shown in Figures 8−10. For example, the formation probability of the pattern surrounded by the dashed square in Figure 10 can be described as $P_a \cdot Q_{1A} \cdot P_a \alpha \gamma / (P_a \alpha \gamma + P_b + P_a \alpha \beta)$ = $P_a{}^2 Q_{1A} \alpha \gamma / (P_a \alpha \gamma + P_b + P_a \alpha \beta)$. These equations can reproduce the site selectivity and the pattern-formation probability for each type of pattern shown in Figures 5 and 7.

Adjusting the parameters of α, β, γ, and δ can reproduce both the site selectivity and the pattern formation well, as shown in Figures 5 and 7. To determine the best parameters of α, β, γ, and δ, it is necessary that these parameters can

reproduce not only the site selectivity but also each pattern formation. If we set $\beta = \gamma$ as in ref 52, the present experimental data cannot be reproduced. The best parameters reproducing the experimental data can suggest the following adsorption physics. (1) $\alpha = 0.48$: This value suggests that the adsorption probability on an adatom depends strictly on the number of adjacent REAs. (2) $\beta = 0.85$: The interaction between the adsorbates on the CEAs is slightly repulsive, and/or the LDOS change on the CEA is not preferred for the adsorption. (3) $\gamma = 2.3$: The interaction between the adsorbates on the CEA and its nearest COAs is strongly attractive, and/or the LDOS change on the adatom is strongly preferred for the adsorption. (4) $\delta = 0.85$: The selection of the configuration P in Figure 3 is preferred due to the possible dipole−dipole interaction of two adsorbates.

We proceeded with investigating the relative preferences of different combinations of adsorbates, consisting of two or three CH_3CN molecules, by analyzing their adsorption energy using DFT calculations. To assess the stability of the adsorption configurations, we calculate the adsorption energies of acetonitriles on the Si{111}-(7 × 7) surface. The adsorption energy (E_{ads}) per acetonitrile is defined as follows
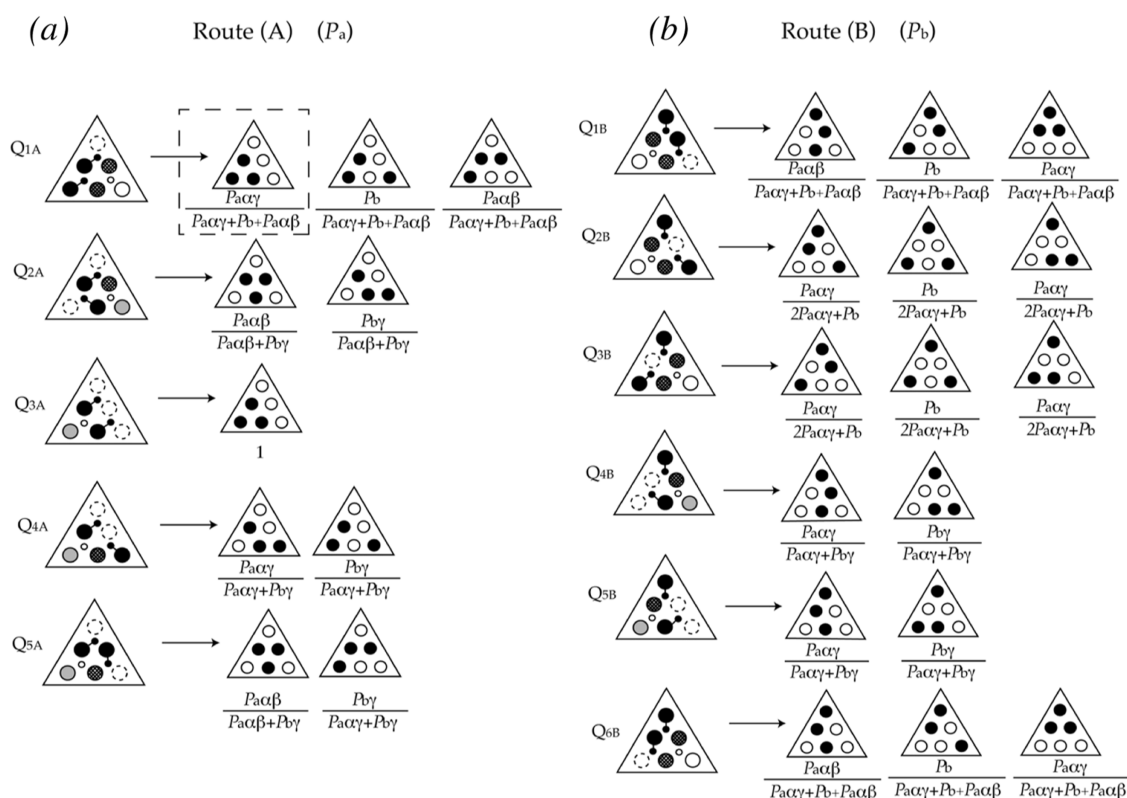
Figure 10. (a) Pattern formation probability of the reacted Si adatoms for the occupations corresponding to the saturation of CH$_3$CN in route (A). (b) Formation probability of patterns of the reacted Si adatoms for occupations corresponding to the saturation of CH$_3$CN in route (B). The leftmost column corresponds to the patterns completed in Figure 9. The right patterns correspond to the saturated patterns of the reacted Si adatoms produced from the most left patterns. The formation probability of each pattern from the most left pattern is shown below the pattern.

Table 1. Adsorption Type and Corresponding Configurations of Two Acetonitrile Molecules[a]

adsorption type	configurations (combination of sites)						E_{ads} (eV)	relative preference
type 2A	2−5	3−6	5−8	6−9	8−2	9−3	1.58	1
type 2A*	2−6	3−8	5−9				1.54	
type 2B	1−4	4−7	7−1				1.46	4
type 2C	1−3	2−4	4−6	5−7	7−9	8−1	1.54	2
type 2D	1−5	1−6	4−9	4−8	7−2	7−3	1.50	3

[a]Their molecular adsorption energies per acetonitrile and relative preference of stability.

Table 2. Adsorption Type and Corresponding Configurations of Three Acetonitrile Molecules[a]

adsorption type	configurations (combination of sites)						E_{ads} (eV)	relative preference I	relative preference II
type 3A	1−4−7						1.45	5	5
type 3B	2−5−8	3−6−9					1.59	1	3
type 3C	1−3−8	2−4−6	7−5−9				1.58	2	2
type 3D	1−3−6	1−8−5	4−6−9	4−2−8	7−5−2	7−9−3	1.57	3	1
type 3E	1−3−7	1−5−7	4−6−1	4−8−1	7−9−4	7−2−4	1.52	4	4

[a]Their molecular adsorption energies per acetonitrile and relative preference of stability.

$$E_{ads} = -[E_{acetonitriles/Si\{111\}-(7\times7)} - E_{Si\{111\}-(7\times7)}$$
$$- nE_{acetonitrile}]/n$$

where $E_{acetonitriles/Si\{111\}-(7\times7)}$, $E_{Si\{111\}-(7\times7)}$, and $E_{acetonitrile}$ represent total energies of the acetonitriles on the Si{111}-(7 × 7) surface, the clean Si{111}-(7 × 7) surface, and the isolated acetonitrile molecule, respectively. Here, n indicates the number of adsorbed acetonitrile molecules.

For the examination of possible molecular adsorption sites of CH$_3$CN on the Si{111}-(7 × 7) unit cell, Figure S1 illustrates

these locations along with the positions of adatoms and rest atoms. The left and right halves of Figure S1 are faulted and unfaulted haves, respectively: the adatoms (green) are labeled by a, b, c, d, e, and f, while the rest atoms (purple) are labeled by g, h, and i. We have a total of nine potential sites for molecular adsorption, denoted as 1 to 9. The CH$_3$CN molecule on each site is adsorbed on the nearest adatom and the nearest rest atom. That is, CH$_3$CN on site 1 is located on the COA a and the REA g, CH$_3$CN on site 2 is on the CEA b and the REA g, CH$_3$CN on site 3 is on the CEA b and the

REA h, etc. These sites are overall categorized into two groups: sites 1, 4, and 7 belong to one group (G1), and sites 2, 3, 5, 6, 8, and 9 belong to the other group (G2). Calculations show that the molecular adsorption energies for the G1 and G2 groups are 1.47 and 1.54 eV, respectively.

If the adsorption of two molecules is considered, we have four types of adsorption configurations, as shown in Table 1. Type 2A has two kinds denoted here by type 2A and type 2A* of which have very close adsorption energies (Table 1). Considering the number of configurations giving the same pattern, the relative preference of stability is in order of type 2A, type 2C, type 2D, and type 2B (see the column for "Relative preference" of Table 1). Thus, our calculations explain the experimental finding to show the trend for the population of the adsorption pattern shown in Figure 7a.

For the adsorption of three molecules, we have five types of adsorption configurations, as shown in Table 2. Considering the number of configurations giving the same pattern, the relative preference of stability is in order of type 3D, type 3C, type 3B, type 3E, and type 3A (see the column for "Relative preference II" of Table 2). Note that without counting the number of configurations, the order of stability follows that of adsorption energy (see the column for "Relative preference I" of Table 2). It is concluded that our calculations (i.e., Relative preference II), taking both the adsorption energy and the number of configurations into account, explain the experimental finding to show the trend for the population of adsorption patterns shown in Figure 7b.

It is worth extracting the intermolecular interactions from the DFT results by subtracting each adsorption energy of a single acetonitrile molecule from the adsorption energy of two or three acetonitrile molecules. As a result, we obtain intermolecular interaction energies of about 0.07 and 0.06 eV for type 2A and type 2C configurations, respectively, of two acetonitrile adsorptions at the nearest distances. In addition, we obtain intermolecular interaction energies of about 0.06 eV for type 3C and 0.05 eV for type 3B and type 3D configurations of the three-acetonitrile adsorption at the nearest distances.

4. SUMMARY

The adsorption of a polarized CH_3CN on Si{111}-(7 × 7) at ~300 K was studied with STM, TDS, and theoretical calculations. The site-specific study enabled us to elucidate the site-by-site and step-by-step adsorption kinetics. A polarized CH_3CN adsorbs preferentially on the faulted half compared to the unfaulted half. Furthermore, the adsorption on the CEA-REA pair is four times preferred to that at the COA-REA pair in each half-unit cell at the initial stage. The site selectivity and also the occurrence of the adsorption pattern are reproduced well by considering the simple model of the probability for each pattern formation. The site-selective adsorption of CH_3CN on Si{111}-(7 × 7) is understood well by the chemical reactivity determined by the local conformation, the local density of states, and the interaction between polarized adsorbates. Detailed theoretical calculations reproduced the experimentally observed patterns of reacted adatoms and supported the interpretations of the reactivity of CH_3CN on Si{111}.

■ ASSOCIATED CONTENT

ⓢ Supporting Information

The Supporting Information is available free of charge at https://pubs.acs.org/doi/10.1021/acsomega.3c05604.

> CH_3CN adsorption sites on the Si{111}-(7 × 7) unit cell shown along with the locations of adatoms and rest atoms (PDF)

■ AUTHOR INFORMATION

Corresponding Authors

Suklyun Hong — *Department of Physics, Graphene Research Institute and GRI-TPC International Research Center, Sejong University, Seoul 143-747, Korea;* ⓞ orcid.org/0000-0001-6504-9209; Email: hong@sejong.ac.kr

Michio Okada — *Institute for Radiation Sciences and Department of Chemistry, Graduate School of Science, Osaka University, Toyonaka, Osaka 560-0043, Japan;* ⓞ orcid.org/0000-0002-7689-4288; Email: okada@chem.sci.osaka-u.ac.jp

Authors

Hironori Mizutani — *Institute for Radiation Sciences and Department of Chemistry, Graduate School of Science, Osaka University, Toyonaka, Osaka 560-0043, Japan*

Hyeong-Kyu Choi — *Department of Physics, Graphene Research Institute and GRI-TPC International Research Center, Sejong University, Seoul 143-747, Korea*

Jinwoo Park — *Department of Physics, Graphene Research Institute and GRI-TPC International Research Center, Sejong University, Seoul 143-747, Korea*

Complete contact information is available at: https://pubs.acs.org/10.1021/acsomega.3c05604

Notes

The authors declare no competing financial interest.

■ ACKNOWLEDGMENTS

■ REFERENCES

(1) Maboudian, R. Surface processes in MEMS technology. *Surf. Sci. Rep.* **1998**, *30*, 207−269.

(2) Yates, J. T. A New Opportunity in Silicon-Based Microelectronics. *Science* **1998**, *279*, 335−336.

(3) Wolkow, R. A. Controlled Molecular Adsorption on Silicon: Laying a Foundation for Molecular Devices. *Annu. Rev. Phys. Chem.* **1999**, *50*, 413−441.

(4) Hamers, R. J.; Coulter, S. K.; Ellison, M. D.; Hovis, J. S.; Padowitz, D. F.; Schwartz, M. P.; Greenlief, C. M.; Russell, J. N. Cycloaddition Chemistry of Organic Molecules with Semiconductor Surfaces. *Acc. Chem. Res.* **2000**, *33*, 617−624.

(5) Filler, M. A.; Bent, S. F. The surface as molecular reagent: organic chemistry at the semiconductor interface. *Prog. Surf. Sci.* **2003**, *73*, 1−56.

(6) Tao, F.; Xu, G. Q. Attachment Chemistry of Organic Molecules on Si(111)-7 × 7. *Acc. Chem. Res.* **2004**, *37*, 882−893.

(7) Tao, F.; Bernasek, S. L.; Xu, G. Q. Electronic and Structural Factors in Modification and Functionalization of Clean and Passivated Semiconductor Surfaces with Aromatic Systems. *Chem. Rev.* **2009**, *109*, 3991−4024.

(8) Teplyakov, A. V.; Kong, M. J.; Bent, S. F. Vibrational Spectroscopic Studies of Diels-Alder Reactions with the Si(100)-2 × 1 Surface as a Dienophile. *J. Am. Chem. Soc.* **1997**, *119*, 11100−11101.

(9) Liu, H.; Hamers, R. J. Stereoselectivity in Molecule-Surface Reactions: Adsorption of Ethylene on the Silicon(001) Surface. *J. Am. Chem. Soc.* **1997**, *119*, 7593−7594.

(10) Rochet, F.; Dufour, G.; Prieto, P.; Sirotti, F.; Stedile, F. C. Electronic structure of acetylene on Si(111)-7 × 7: X-ray photo-electron and x-ray absorption spectroscopy. *Phys. Rev. B* **1998**, *57*, 6738−6748.

(11) Hamaguchi, K.; Machida, S.; Mukai, K.; Yamashita, Y.; Yoshinobu, J. Adsorption state of 1,4-cyclohexadiene on Si(100) (2 × 1). *Phys. Rev. B* **2000**, *62*, 7576−7580.

(12) Pecher, L.; Mette, G.; Dürr, M.; Tonner, R. Site-Specific Reactivity of Ethylene at Distorted Dangling-Bond Configurations on Si(001). *ChemPhysChem* **2017**, *18*, 357−365.

(13) Qiao, M. H.; Tao, F.; Cao, Y.; Li, Z. H.; Dai, W. L.; Deng, J. F.; Xu, G. Q. Cycloaddition reaction of furan with Si(100)-2 × 1. *J. Chem. Phys.* **2001**, *114*, 2766−2774.

(14) Lee, H.-K.; Park, J.; Kim, K.-J.; Kim, H.-D.; Lee, I.-J.; Shin, H.-J.; Kim, B.; Yu, B. D.; Hong, S.; Chung, J. Enhanced Deseleniumization of Selenophene Molecules Adsorbed on Si(100)-2 × 1 Surface. *J. Phys. Chem. C* **2011**, *115*, 17856−17860.

(15) Park, J.; Lee, H.-K.; Soon, A.; Yu, B. D.; Hong, S. Thermally Induced Desulfurization: Structural Transformation of Thiophene on the Si(100) Surface. *J. Phys. Chem. C* **2013**, *117*, 11731−11737.

(16) Hovis, J. S.; Hamers, R. J. Structure and Bonding of Ordered Organic Monolayers of 1,5-Cyclooctadiene on the Silicon(001) Surface. *J. Phys. Chem. B* **1997**, *101*, 9581−9585.

(17) Ferraz, A.; Miotto, R. A comparative study of the interaction of cyclopentene, cyclohexene, and 1,4-cyclohexadiene with the silicon surface. *Surf. Sci.* **2004**, *566−568*, 713−718.

(18) Taguchi, Y.; Fujisawa, M.; Takaoka, T.; Okada, T.; Nishijima, M. Adsorbed state of benzene on the Si(100) surface: Thermal desorption and electron energy loss spectroscopy studies. *J. Chem. Phys.* **1991**, *95*, 6870−6876.

(19) Schwartz, M. P.; Ellison, M. D.; Coulter, S. K.; Hovis, J. S.; Hamers, R. J. Interaction of π-Conjugated Organic Molecules with π-Bonded Semiconductor Surfaces: Structure, Selectivity, and Mechanistic Implications. *J. Am. Chem. Soc.* **2000**, *122*, 8529−8538.

(20) Guo, S. Y.; Timm, M. J.; Huang, K.; Polanyi, J. C. Electron Attachment Leads to Unidirectional In-Plane Molecular Rotation of Para-Chlorostyrene on Si(100). *J. Phys. Chem. C* **2019**, *123*, 18425−18431.

(21) Flammini, R.; Cecchetti, D.; Tagliatesta, P.; Carbone, M. Multiple options for phenol on Si(111)7 × 7 revealed by high resolution photoemission. *Surf. Sci.* **2020**, *692*, 121510.

(22) Tao, F.; Wang, Z. H.; Qiao, M. H.; Liu, Q.; Sim, W. S.; Xu, G. Q. Covalent attachment of acetonitrile on Si(100) through Si-C and Si-N linkages. *J. Chem. Phys.* **2001**, *115*, 8563−8569.

(23) Bournel, F.; Gallet, J.-J.; Kubsky, S.; Dufour, G.; Rochet, F.; Simeoni, M.; Sirotti, F. Adsorption of acetonitrile and acrylonitrile on Si-2×1 at room temperature studied by synchrotron radiation photoemission and NEXAFS spectroscopies. *Surf. Sci.* **2002**, *513*, 37−48.

(24) Mui, C.; Filler, M. A.; Bent, S. F.; Musgrave, C. B. Reactions of Nitriles at Semiconductor Surfaces. *J. Phys. Chem. B* **2003**, *107*, 12256−12267.

(25) Cho, J. H.; Kleinman, L. *Ab initio* calculations of the adsorption and reaction of acetonitrile on Si(001). *J. Chem. Phys.* **2003**, *119*, 6744−6749.

(26) Miotto, R.; Oliveira, M. C.; Pinto, M. M.; de Leon-Perez, F.; Ferraz, A. C. Acetonitrile adsorption on Si(001). *Phys. Rev. B* **2004**, *69*, 235331.

(27) Rezaei, M. A.; Stipe, B. C.; Ho, W. Atomically resolved adsorption and scanning tunneling microscope induced desorption on a semiconductor: NO on Si(111)-(7 × 7). *J. Chem. Phys.* **1999**, *110*, 4891−4896.

(28) El Garah, M.; Makoudi, Y.; Cherioux, F.; Duverger, E.; Palmino, F. Chemisorption of Trimesic Acid on a Si(111)-7 × 7 Surface. *J. Phys. Chem. C* **2010**, *114*, 4511−4514.

(29) Guan, D.; Wang, X.; Mao, H.; Bao, S.; Jia, J.-F. Adsorption of Perylene on Si(111)(7 × 7). *Chin. Phys. Lett.* **2020**, *37*, 027101.

(30) Jarvis, S. P.; Sweetman, A. M.; Lekkas, I.; Champness, N. R.; Kantorovich, L.; Moriarty, P. Simulated structure and imaging of NTCDI on Si(111)-7 × 7: a combined STM, NC-AFM and DFT study. *J. Phys.: Condens. Matter* **2015**, *27*, 054004.

(31) Makoudi, Y.; Arab, M.; Palmino, F.; Duverger, E.; Ramseyer, C.; Picaud, F.; Chérioux, F. A Stable Room-Temperature Molecular Assembly of Zwitterionic Organic Dipoles Guided by a Si(111)-7 × 7 Template Effect. *Angew. Chem., Int. Ed.* **2007**, *46*, 9287−9290.

(32) Makoudi, Y.; Arab, M.; Palmino, F.; Duverger, E.; Ramseyer, C.; Picaud, F.; Chérioux, F. A Stable Room-Temperature Molecular Assembly of Zwitterionic Organic Dipoles Guided by a Si(111)-7×7 Template Effect. *Surf. Sci.* **2007**, *46*, 9287−9290.

(33) Utecht, M.; Gaebel, T.; Klamroth, T. Desorption induced by low energy charge carriers on Si(111)-7 × 7: First principles molecular dynamics for benzene derivates. *J. Comput. Chem.* **2018**, *39*, 2517−2525.

(34) Lock, D.; Sakulsermsuk, S.; Palmer, R. E.; Sloan, P. A. Mapping the site-specific potential energy landscape for chemisorbed and physisorbed aromatic molecules on the Si(111)-7 × 7 surface by time-lapse STM. *J. Phys.: Condens. Matter* **2015**, *27*, 054003.

(35) Motevalli, B.; Taherifar, N.; Wu, B.; Tang, W.; Liu, J. Z. A density functional theory computational study of adsorption of Di-Meta-Cyano Azobenzene molecules on Si (111) surfaces. *Appl. Surf. Sci.* **2017**, *422*, 557−565.

(36) Mararov, V. V.; Gruznev, D. V.; Bondarenko, L. V.; Tupchaya, A. Y.; Zotov, A. V.; Saranin, A. A. Comparative STM analysis of C_{60} and C_{70} fullerene adsorption sites on pristine and Al-modified Si(111)7 × 7 surfaces. *J. Vac. Sci. Technol., A* **2016**, *34*, 061402.

(37) Shimomura, M.; Iwanabe, A.; Kiyose, T. Dynamic Observation of Confined Molecules in Self-Assembled Molecular Corrals. *J. Phys. Chem. C* **2014**, *118* (47), 27465−27469.

(38) Takayanagi, K.; Tanishiro, Y.; Takahashi, M.; Takahashi, S. Structural analysis of Si(111)-7 × 7 by UHV-transmission electron diffraction and microscopy. *J. Vac. Sci. Technol., A* **1985**, *3*, 1502−1506.

(39) Neergaard Waltenburg, H.; Yates, J. T. Surface Chemistry of Silicon. *Chem. Rev.* **1995**, *95*, 1589−1673.

(40) *CRC Handbook of Chemistry and Physics*; 68th edn; Haynes, W. H., Ed.; Chemical Rubber Company: Boca Raton, FL, 1987.

(41) Tao, F.; Chen, X. F.; Wang, Z. H.; Xu, G. Q. Binding and Structure of Acetonitrile on Si(111)-7 × 7. *J. Phys. Chem. B* **2002**, *106*, 3890−3895.

(42) Bournel, F.; Carniato, S.; Dufour, G.; Gallet, J. J.; Ilakovac, V.; Rangan, S.; Rochet, F.; Sirotti, F. Adsorption of acetonitrile (CH_3CN) on Si(111)-7 × 7 at room temperature studied by synchrotron radiation core-level spectroscopies and excited-state density functional theory calculations. *Phys. Rev. B* **2006**, *73*, 125345.

(43) Hong, S.; Min, K.-A.; Park, J.; Kim, H.; Mizutani, H.; Okada, M. Adsorption of Acetonitrile on Si(111)-(7 × 7). *ACS Omega* **2020**, *5*, 24179−24185.

(44) Kresse, G.; Furthmüller, J. Efficient iterative schemes for *ab initio* total-energy calculations using a plane-wave basis set. *Phys. Rev. B* **1996**, *54*, 11169−11186.

(45) Kresse, G.; Furthmüller, J. Efficiency of ab-initio total energy calculations for metals and semiconductors using a plane-wave basis set. *Comput. Mater. Sci.* **1996**, *6*, 15−50.

(46) Perdew, J. P.; Burke, K.; Ernzerhof, M. Generalized Gradient Approximation Made Simple. *Phys. Rev. Lett.* **1996**, *77*, 3865−3868.

(47) Blöchl, P. E. Projector augmented-wave method. *Phys Rev B Condens Matter.* **1994**, *50*, 17953−17979.

(48) Kresse, G.; Joubert, D. From ultrasoft pseudopotentials to the projector augmented-wave method. *Phys. Rev. B* **1999**, *59*, 1758−1775.

(49) Grimme, S.; Antony, J.; Ehrlich, S.; Krieg, H. A consistent and accurate *ab initio* parametrization of density functional dispersion correction (DFT-D) for the 94 elements H-Pu. *J. Chem. Phys.* **2010**, *132*, 154104.

(50) Lu, X.; Wang, X.; Yuan, Q.; Zhang, Q. Diradical Mechanisms for the Cycloaddition Reactions of 1,3-Butadiene, Benzene, Thiophene, Ethylene, and Acetylene on a Si(111)-7 × 7 Surface. *J. Am. Chem. Soc.* **2003**, *125*, 7923−7929.

(51) From our thermal-desorption experiments in Figure 2, CH_3CN molecules are desorbed below 650 K. Thus, the STM image in Figure 6 of ref 43 corresponds to the dissociated species.

(52) Tanaka, K.; Xie, Z. X. Adsorption kinetics and patterning of a Si(111)-7 × 7 surface by dissociation of methanol. *J. Chem. Phys.* **2005**, *122*, 054706.